A&A 626, A107 (2019)
https://doi.org/10.1051/0004-6361/201834727

Astronomy & Astrophysics

Dust trajectory simulations around the Sun, Vega, and Fomalhaut

Johann Stamm[1], Andrzej Czechowski[2], Ingrid Mann[1], Carsten Baumann[1], and Margaretha Myrvang[1]

[1] Department of Physics and Technology, University of Tromsø, Tromsø, Norway
e-mail: j.research@stamm.no
[2] Space Research Centre, Polish Academy of Sciences, Warsaw, Poland

Received 27 November 2018 / Accepted 25 April 2019

ABSTRACT

Context. Vega and Fomalhaut display a thermal emission brightness that could possibly arise from hot dust near the stars, an inner extension of their planetary debris disks. An idea has been suggested that nanometer-sized dust particles are kept in the vicinity of the stars by electromagnetic forces. This resembles the trapping that model calculations show in the corotating magnetic field in the inner heliosphere within approximately 0.2 AU from the Sun.
Aims. The aim of this work is to study whether the trapping of dust due to electromagnetic forces acting on charged dust near the Sun can occur around Vega and Fomalhaut and what are the conditions for trapping.
Methods. We studied the dust trajectories with numerical calculations of the full equation of motion, as well as by using the guiding center approximation. We assumed a constant dust charge and a Parker-type magnetic field, which we estimated for the two stars.
Results. We find no bound trajectories of charged particles around Vega or Fomalhaut as long as the radiation pressure force exceeds the gravitational force, that is, for particles smaller than 1 μm. A trapping zone could exist inside of 0.02 AU for Vega and 0.025 AU for Fomalhaut, but only for those particles with radiation pressure force smaller than gravitational force. In comparison to the Sun, the trapping conditions would occur closer to the stars because their faster rotation leads to a more closely wound-up magnetic field spiral. We also show that plasma corotation can be consistent with trapping. Our model calculations show that the charged particles are accelerated to stellar wind velocity very quickly, pass 1 AU after approximately three days, and are further ejected outward where they pass the debris disks at high velocity. We find this for particles with a surface charge-to-mass ratio larger than 10^{-6} elementary charges per proton mass for both negatively and positively charged dust and independent of the strength of the radiation pressure force. Based on charging assumptions, this would correspond to dust of sizes 100 nm and smaller.

Key words. interplanetary medium – solar wind – acceleration of particles – stars: magnetic field – methods: numerical

1. Introduction

The vicinity of the Sun overlaps with the inner region of the solar system's zodiacal cloud, which is made up of dust particles that form over a large interval of sizes by the collisional fragmentation of asteroids, objects emitted from comets, and smaller fragment of these objects. Planetesimals likewise produce dust in extrasolar planetary systems so that many main-sequence stars are surrounded by dusty debris disks. The dusty debris disks were first noticed in infrared observations, where the dust emission generates an excess brightness in comparison to the stellar spectrum. Most observational results describe cold and warm dust components at large distances from the stars comparable to regions beyond the asteroid belt and beyond the Kuiper belt of the solar system (cf. e.g., Wyatt 2009; Moro-Martin 2013).

Observational constrains usually prevent the detailed investigation of the innermost parts of the debris disks, because the hot dust emission overlaps with the brightness of the star and because of a lack of spatially resolved observations, an exception being recent interferometric studies (Absil et al. 2013; Ertel et al. 2016). At the same time, the inner debris disks are an interesting target of studies, since they have an impact on the evolution of the whole disk. The dust that is accelerated close to the star passes the outer disk where it enhances the collision rate and changes the dust distribution (cf. e.g., Czechowski & Mann 2007; Sezestre et al. 2017). The dust fluxes are also of special interest because the inner debris disks overlap with the hypothesized habitable zones (cf. e.g., Lammer et al. 2009) around the stars, and dust fluxes possibly have an influence on the evolution of the atmospheres of planets that could be located in this region.

The dust dynamics in the inner debris disks was in particular brought up in a recent study of the A-type stars Vega and Fomalhaut motivated by observational results with near infrared interferometry. Observations suggest that dust is likely to exist in the close vicinity of Vega (Absil et al. 2006) and a model to explain Vega observations suggests a component of small dust at about 0.1–0.3 AU around the star (Defrère et al. 2011). Observations also suggest the existence of hot dust particles within 6 AU from Fomalhaut (Absil et al. 2009). A work by Lebreton et al. (2013) suggests that the dust has a high temperature, is located close to the star, and includes a population of very small dust with sizes 10–500 nm at distances of 0.1–0.3 AU as well as a ring around 2 AU from the star. In a comparison of the disks around Vega and Fomalhaut, which is based on a number of different observations, Su et al. (2013) investigate the hot dust emission and as a possible scenario for its origin suggest the trapping of nanodust particles by electromagnetic forces, a process that was shown with trajectory calculation for the vicinity of the Sun (Czechowski & Mann 2010).

In the limit of nanometer-sizes, dust particles are most strongly deflected in the solar wind, in a process similar to the formation of solar wind pick up ions (Mann et al. 2007). While this normally leads to the ejection of particles, under certain

conditions the nanodust has a trapping-like motion near the Sun (Czechowski & Mann 2010). Based on the guiding center approximation, the motion can be described as the sliding along a rotating solar magnetic field line. In this simplified view, the sliding along the field line is determined by the combination of the magnetic mirror force, solar gravity, and a term that is analogous to the centrifugal force (Czechowski & Mann 2010). Su et al. (2013) suggested that this trapping also occurs around Vega and Fomalhaut and gives rise to their hot debris disks. Since it is a possible mechanism that explains the existence of the hot disks, it is of interest to study the trapping.

In this article, we study the dynamics of charged dust particles around Vega, Fomalhaut, and close to the Sun in order to investigate under what conditions the suggested trapping can occur, and we characterize the motion of non-trapped particles. The text is organized as follows. In Sect. 2 the magnetic field model is described. The equation of motion is also described here. The method of calculations and guiding center approximation is described in Sect. 3. The results of the trajectory simulations of particles around the Sun and around Vega and Fomalhaut are described in Sects. 4 and 5, respectively. In Sect. 6, we improve the magnetic field model to include corotation of plasma close to the star. Finally, the conclusions are drawn in Sect. 7.

2. Acting forces and equation of motion

Dust particles move within the gravitational, radiation, and magnetic field of the star. For the magnetic field in the solar wind region, a Parker spiral model (Parker 1958) is often assumed. This model is a good description for the structure of the magnetic field when the frozen-in condition applies. An initially radial magnetic field at the solar surface is convected outward with the radially moving solar wind. The frozen-in effect together with the rotation of the Sun causes the spiral shape of the magnetic field. The polarity of a field line at a certain point is determined by the direction of the dipole component of the solar magnetic field at the footpoint of the field line. The version of the model used in most of the calculations reported here is the same as in Czechowski & Mann (2010). The solar wind is assumed to be radially directed and the speed to be constant, 400 km s^{-1} at a latitude below 20°($|\theta - 90°| \leq 20°$) and 800 km s^{-1} at a latitude above 20°($|\theta - 90°| > 20°$). The magnetic field at a distance r from the Sun is

$$\boldsymbol{B} = \tilde{B}_r \left(\frac{\bar{r}}{r}\right)^2 (\hat{\boldsymbol{r}} - ar\hat{\boldsymbol{\varphi}}), \tag{1}$$

where $\tilde{B}_r$ is the magnetic field strength in radial direction at $r = \bar{r} = 1$ AU, $\hat{\boldsymbol{r}}$ is the unit radial vector, $\hat{\boldsymbol{\varphi}}$ is the unit azimuthal angle vector for $\varphi \in [0, 360°]$, and

$$a = \frac{\Omega \sin\theta}{u}, \tag{2}$$

where Ω is the solar rotation velocity and u is the solar wind speed at solar colatitude $\theta \in [0°, 180°]$. The solar wind speed is assumed to be independent of the distance from the Sun. This approximation is not very useful close to the Sun and we will consider a radial dependent wind profile in Sect. 6. The solar rotation is assumed to be the same for all latitudes.

Equation (1) is valid as long as $r \gg R_\odot$, where $R_\odot$ is the radius of the Sun. Otherwise, the solar wind velocity is not purely radial and the azimuthal magnetic field becomes affected. The model is therefore applicable outside of the Alfvén radius, which is estimated at about 0.1 AU (20 $R_\odot$) (Schatten et al. 1969).

The magnitude of $\tilde{B}_r$ is given by

$$\left|\tilde{B}_r\right| = \frac{\tilde{B}}{\sqrt{\bar{a}^2 + 1}}, \tag{3}$$

where $\tilde{B} = \tilde{B}_\odot = 5$ nT (50 μG) is the magnetic field strength at 1 AU and near the ecliptic and $\bar{a} = \Omega\bar{r}/u$. Our specification of the magnetic field in terms of its strength at 1 AU is the same as used in Czechowski & Mann (2012). We keep the same convention also for the cases of Vega and Fomalhaut.

The sign of $\tilde{B}_r$ is decided by the sign of $\boldsymbol{r} \cdot \boldsymbol{d}$, where $\boldsymbol{d}$ is the direction of the solar dipole at time $t' = t - r/u$ when the corresponding plasma volume left the solar surface. In all calculations, the solar dipole is aligned with the solar rotation. This implies that $\boldsymbol{d} = \pm\hat{\boldsymbol{z}}$ and is independent from time. The boundary between slow and fast solar wind was set to a latitude of 20°. Both the magnetic and the rotational solar equator are assumed to lie in the ecliptic. The magnetic field of the Sun can either be in a focusing or antifocusing configuration. In the focusing configuration the magnetic field in the northern hemisphere points toward the Sun (Czechowski & Mann 2010). The antifocusing magnetic field points in the opposite direction. All results shown here use a focusing magnetic field if not stated otherwise.

Knowledge on the magnetic fields of Vega and Fomalhaut is sparse. For Vega, the magnetic field is known from observations of the surface that points towards Earth (Lignières et al. 2009). Vega is almost seen pole-on, the stellar rotation axis is tilted ~5° relative to its direction towards the Sun (Yoon et al. 2010). This tilt will be neglected further on. The strength of the magnetic field in the direction of the Earth averaged over the surface pointing towards Earth, $\langle B_z \rangle$, is -60 ± 30 μT (Lignières et al. 2009).

We assume that the magnetic field close to Vega and Fomalhaut can be described with the Parker model. In order to estimate the strength, we compared it to the conditions around the Sun. We extrapolated the Parker model to the solar surface and took the scalar product of the magnetic field with the polar unit vector, $\hat{z}$, to obtain the magnetic field pointing in polar direction at the surface (B_z):

$$B_z = \tilde{B}_\mathrm{V} \frac{\cos\theta}{\sqrt{\bar{a}^2 + 1}} \left(\frac{\bar{r}}{r}\right)^2, \tag{4}$$

where $\tilde{B}_\mathrm{V}$ is the magnetic field strength of Vega at 1 AU. We can average this expression over the northern hemisphere, that is, the upper half of the stellar surface. Assuming that the surface of the star is spherical and that stellar wind is constant at all latitudes, we get

$$\langle B_z \rangle = \frac{\tilde{B}_\mathrm{V} \bar{r}^2}{2R_\mathrm{V}^2 \sqrt{\left(\frac{\Omega_\mathrm{V}\bar{r}}{u_\mathrm{V}}\right)^2 + 1}}. \tag{5}$$

We assume that the stellar wind speed of Vega is equal to the escape speed at the surface equator. Using stellar parameters from Table 1, we estimate the magnetic field strength of Vega at 1 AU to be $\tilde{B}_\mathrm{V} = 687$ nT, this is 137 times the same value for the Sun. The magnetic field strength of Fomalhaut we estimate by regression using Sun and Vega as a basis. Also for Fomalhaut, the stellar wind speed is assumed to be equal to the escape speed at the surface. The independent variables are radius squared, mass, rotation, and age. For the radius, we use both equatorial and polar values.

Table 1. Parameters of Sun, Vega, and Fomalhaut.

Star	Sun	Vega	Fomalhaut
Distance	–	7.76 pc [4]	7.70 pc [6]
Radius	$1\ R_\odot = 6.957 \times 10^8$ m [1] (0.00465 AU)	2.818 $R_\odot$ [a] [5] (0.0131 AU [a]) 2.362 $R_\odot$ [b] [5]	1.842 $R_\odot$ [6] (0.00857 AU)
Gravitation constant × Mass	$1\ GM_\odot = 1.3271 \times 10^{20}$ 1 ms^{-2} [1]	2.135 $GM_\odot$ [5]	1.92 $GM_\odot$ [6]
Rotation speed	2.86×10^{-6} rad s^{-1} [c] [2]	1.20×10^{-4} rad s^{-1} [a] [5]	7.76×10^{-5} rad s^{-1} [a,d] [6]
Escape speed [a,d]	6.1×10^5 m s^{-1}	5.4×10^5 m s^{-1}	6.3×10^5 m s^{-1}
Age	4.57×10^9 yr [3]	455×10^6 yr [4]	440×10^6 yr [6]

Notes. The rotation speed of Fomalhaut is only measured projected onto the line of sight. The value in the table is calculated by the assumption that the equator of Fomalhaut lies in the plane of its outer debris disk, which has an inclination of 67° (Su et al. 2013). [a]At equator. [b]At the poles. [c]At 26° latitude. [d]Calculated.

References. [1]IAU (2015); [2]Hakamada & Kojima (1994); [3]Bonanno et al. (2002); [4]Köhler & Mann (2002); [5]Yoon et al. (2010); [6]Mamajek (2012); [7]Díaz et al. (2011).

Table 2. Results of magnetic field strength estimation of Fomalhaut.

Independent variable	In units of	Magnetic field strength of Fomalhaut ($\tilde{B}_\mathrm{F}$)
Equatorial radius squared	solar radii	64 $\tilde{B}_\odot$
Polar radius squared	solar radii	85 $\tilde{B}_\odot$
Mass	solar masses	111 $\tilde{B}_\odot$
Age	yr	137 $\tilde{B}_\odot$
Rotation speed	rad s^{-1}	86 $\tilde{B}_\odot$

The results of the magnetic field strength estimation shown in Table 2 show that the strength of the magnetic field of Fomalhaut varies strongly with the selection of the independent variable. Braithwaite & Cantiello (2013) predict that the magnetic field strength is dependent on at least the age and rotation speed of the star. These two variables give a magnetic field strength for Fomalhaut that is evenly on each side of the estimate by taking the mass as an independent variable. We therefore choose the mass and hence the magnetic field strength of Fomalhaut at 1 AU is estimated to be 111 times the magnetic field strength of the Sun. This corresponds to a value of 555 nT. Rieke et al. (2016) estimate the Alfvén radius of an A-class reference star to be at 0.19 AU. We assume this Alfvén radius for Vega and Fomalhaut.

We further assume that the magnetic field does not vary in time. A force caused by momentum transfer between the streaming stellar wind particles and the dust particles was considered by Czechowski & Kleimann (2017), but is not considered here. The full equation of motion for the dust particles can then be written as

$$\frac{\mathrm{d}^2\boldsymbol{r}}{\mathrm{d}t^2} = -\frac{GM}{r^2}\hat{\boldsymbol{r}} + \frac{GM}{r^2}\beta\left(\left(1-\frac{v_r}{c}\right)\hat{\boldsymbol{r}} - \frac{\boldsymbol{v}}{c}\right) + \frac{q}{m}(\boldsymbol{v}-\boldsymbol{u})\times\boldsymbol{B}, \quad (6)$$

where G is the gravity constant, M is the stellar mass, r the distance from the star, and β, q, m, and v are the ratio between radiation force and gravity, the charge, the mass, and the velocity of the particle, respectively. Further, v_r is the velocity of the particle in the radial direction, c the speed of light in vacuum, $\boldsymbol{u}$ the stellar wind velocity, and $\boldsymbol{B}$ the magnetic field. This is the same equation of motion as in Czechowski & Mann (2010). They also calculated the specific energy equation for the dust particle,

$$\frac{v^2}{2} - \frac{GM}{r}(1-\beta) - \frac{q\tilde{B}_r}{m}\Omega\bar{r}^2\sin\varphi = \frac{E}{m}, \quad (7)$$

which is approximately constant for uniform stellar wind speed and magnetic field polarity. Since the Poynting-Robertson effect is negligible on the timescales considered here, conservation of this parameter indicates the reliability of the numerical calculations.

3. Solving the equation of motion and trajectory calculations

In the trajectory calculations, we assume that the dust particles are released from a parent body, which moves in a Keplerian orbit. We assume that the fragment particle initially has the same velocity as the parent body. When referring to initial orbit parameters, the orbit parameters of the parent body are meant. The release point is the point in the initial orbit where the dust particle and parent body are separated. In most of our calculations, the particles are released at the highest latitude of the initial orbit, by choosing the argument of periapsis accordingly.

The equation of motion, Eq. (2), is solved numerically by a fourth-order Runge-Kutta solver with variable time step. The initial values for the particles correspond to certain points in Keplerian orbits around the star. The simulation time varies between 3×10^6 s (about 35 days) for the closest particles (6×10^6 s when released outside of the periapsis) and 30×10^6 s for the farthest particles. It is chosen so that the particles could fulfill at least one orbit. The simulation time around Vega and Fomalhaut is always 30×10^6 s. When a particle hits the star, the calculation is interrupted. It is also interrupted when the particle reaches distances outside of 3 AU. In this latter case, the distance variation is inspected to see if the particle has a chance to come back in a reasonable timescale and if so, the trapping is set to undecided.

The initial orbits have different eccentricities, inclinations, and semimajor axes. Also, different starting positions in the orbits were considered. The argument of periapsis was either

0° or 90°, depending on the initial position in the orbit. The longitude of ascending node was always set to zero.

In the equation of motion, the charge and the mass always appear as a ratio. The considered charge-to-mass ratios are 10^{-4}, 10^{-5}, 7×10^{-6}, 5×10^{-6}, 3×10^{-6}, 1×10^{-6}, and 10^{-7} in units of elementary charges per proton mass (q_e/m_p), and assumed to be constant as previously used by Czechowski & Mann (2010). These values correspond to particles with sizes of 3–100 nm in solar wind conditions (Czechowski & Mann 2012). The results of Kimura et al. (2018) show that the charge-to-mass ratio is related to the particle size for the A-class star β Pictoris in the same way as for the Sun. We assume that this will be valid for Vega and Fomalhaut too. In addition, trajectories of neutral particles are considered for comparison.

For particles around the Sun, β is assumed to be 0.1, as in Czechowski & Mann (2010). The β-values for particles around Vega and Fomalhaut are taken to be as low as reasonable. Myrvang (2018) found $\beta \gtrsim 2$ for Vega and $\beta \gtrsim 1$ for Fomalhaut for particles with a size of some μm and smaller. Here, we use $\beta = 2$ if not stated otherwise.

In addition to the numerical calculations, we investigated the trapping conditions by using the guiding center approximation (Northrop 1963). This describes the trajectories as a superposition of gyration about a magnetic field line and motion along the field line. The latter is the motion of the guiding center. This simplifies the radial part of the equation of motion (Northrop 1963; Czechowski & Mann 2010, 2011). We modified the equation from the latter to clarify the velocity dependence by inserting for the magnetic moment, $\mu = (\boldsymbol{v}_\perp - \boldsymbol{u}_\perp)^2/2B$. We note that $\boldsymbol{v}_\perp - \boldsymbol{u}_\perp$ is not constant during guiding center motion. Equation (2) can then be simplified to

$$\frac{\mathrm{d}v_r^G}{\mathrm{d}t} = -\frac{GM(1-\beta)}{r^2h^2} + \frac{(\boldsymbol{v}_\perp - \boldsymbol{u}_\perp)^2}{rh^2}\left(1 - \frac{a^2r^2}{2h^2}\right) + \frac{u^2a^2r}{h^2} - \frac{v_r^{G2}a^2r}{h^2}, \tag{8}$$

where v_r^G is the radial velocity of the guiding center, $\boldsymbol{v}_\perp$ and $\boldsymbol{u}_\perp$ are the velocity of the particle and stellar wind velocity perpendicular to the magnetic field, respectively, and $h = \sqrt{1 + a^2r^2}$. The approximation is valid if the forces on the particle do not vary considerably over one gyroperiod. In Eq. (8), the first term describes the combined gravitation and radiation pressure force. It is directed toward the star when $\beta < 1$ and away from the star when $\beta > 1$. The Poynting-Robertson effect is neglected here. The second term corresponds to the magnetic mirror force, which is caused by the inward converging of the magnetic field lines. It can be shown that this term always points outward. The next term is analogous to the centrifugal force. The motion of the guiding center does not depend on the charge-to-mass ratio.

The perpendicular velocity of the guiding center $v_\perp^G$ we approximate by

$$\boldsymbol{v}_\perp^{\boldsymbol{G}} = \boldsymbol{u}_\perp. \tag{9}$$

In the following we shall use the sign of the initial radial acceleration $\mathrm{d}v_r^G/\mathrm{d}r$ given by Eq. (9) as an approximate criterion for trapping. Using the results of Czechowski & Mann (2010, 2011), it follows that if the initial value of v_r is zero, the negative sign of $\mathrm{d}v_r^G/\mathrm{d}t$ is a sufficient condition for trapping.

The trapping of the uncharged particles only depends on the eccentricity of the initial orbit, the β, and the initial position. The trapping of the charged particles also depends on the distance to the star when released and the inclination of the initial orbit.

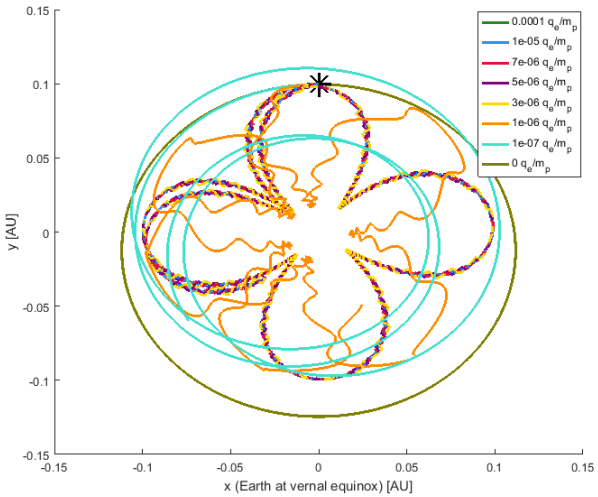

Fig. 1. Trajectories of particles after release. The motion is projected to the ecliptic. The orbits of the particles with a charge-to-mass ratio of $\geq 3\times10^{-6}q_e/m_p$ are overlapping. All trajectories have same initial values. The star (*) marks the initial position of the trajectories. The initial orbit for this simulation is circular, with a radius of 0.1 AU, an inclination of 5°, and an argument of periapsis of 90°; its length of ascending node is 0°and the particles are released in the periapse.

The latitude of release might also contribute to the results (cf. Czechowski & Mann 2010), but is not investigated here.

To check the reliability of the numerical calculations, we consider the specific energy of the particles in the trajectories, Eq. (7). For most trajectory calculations, the parameter is conserved inside of the regions with uniform stellar wind speed and magnetic field polarity.

4. Results of trajectory simulations of particles around the Sun

Our calculations provide the position and velocity of the particles as a function of time. From that we derive additional parameters, including speed, distance, gyroradius, and specific energy of the particle. An example of a trajectory for a trapped particle is shown in Fig. 1.

The calculations of dust trajectories around the Sun can be divided into different groups. One has initial values with varying inclination, one has varying initial eccentricity, and two have varying eccentricity and different positions in the initial orbit. The results for a particle with $q/m = 10^{-4}\ q_e/m_p$ are shown in Fig. 2, where the results are shown for every group. Figure 2a shows the dependence on the initial inclination while the eccentricity is zero for all simulations. In Fig. 2b, the inclination is 5°, while the eccentricity varies. In Fig. 2c, the inclination and eccentricity are as in Fig. 2b, but the particles are released at true anomaly = 90°. The initial orbit is rotated so that the release point still is at the highest latitude. Likewise, in Fig. 2d, but the release point is now set to true anomaly = −90°. In contrast to the others, the release point is at the lowest latitude.

In the figures, the background shows the initial acceleration that is derived using the guiding center approximation. The colors are chosen so that acceleration inward is shown in blue and acceleration outward is shown by the green and sandy colors. The dots show the result of the particle trajectory simulations with full equation of motion.

For the value $\beta = 0.1$ used in these simulations, the particles are in general in bound orbit for $q/m \ll 10^{-7}q_e/m_p$ and the

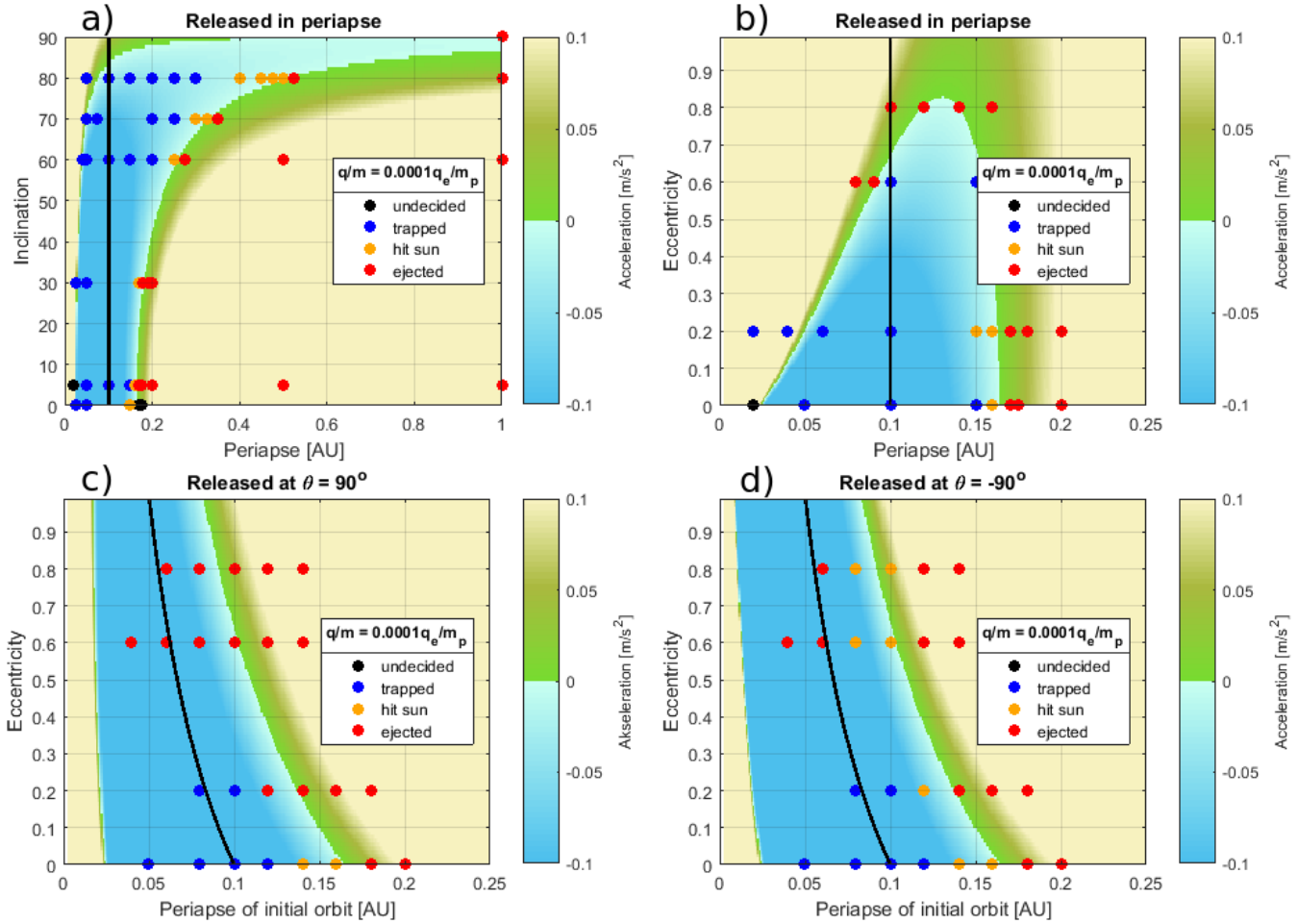

Fig. 2. Results of dust trajectory calculations dust around the Sun with initial orbits with varying inclination (*a*) and eccentricities (*b*–*d*). In (*b*), the starting point is the periapse, in (*c*) it is at $\theta = 90°$ and at $\theta = -90°$ in (*d*). The background shows the initial radial acceleration averaged over one gyroperiod by using the guiding center approximation. Both the *x*- and *y*-axis show values of the initial orbit. The black line shows the Alfvén radius. The points show the results of the numerical simulations with full equation of motion, Eq. (2). Blue means that the particle was trapped, red means that it was ejected, orange means that it hits the Sun, and black means that the result was ambiguous. Since the eccentricity is 0 in (a) and (b), the periapse is equal to the initial distance from the Sun.

guiding center approximation is only applicable when the particles are released in the periapse. The calculations show that for certain initial values, the charged particles are trapped. This region is located inside of 0.2 AU, but extends outward a bit for higher inclinations and heavily charged particles. In the figures, the trapping region can be seen as the part of the background that is blue. An inner boundary of the trapping region might exist, but here the trajectory simulations and the initial acceleration using the guiding center approximation give different results. In addition, this boundary is at distances where the Parker model is not applicable.

The trapping region shrinks even more if the particle is released outside of the periapse (compare Figs. 2a and b to 2c and d). Here the trajectory simulations do not agree with the guiding center approximation. A reason for this could be that by using the approximation only the initial radial acceleration was considered.

The further from the Sun the particle starts in the trapping region, the closer it comes to the Sun. Some particles come so close that they hit the Sun and the calculation is interrupted. Interestingly, this happens mostly for particles starting at the outer border of the trapping region (cf. Czechowski & Mann 2012).

5. Particle trajectories around Vega and Fomalhaut

We see that in Fig. 2 the ejection of the particles is predicted well by the initial acceleration of the dust particles, which we obtain using the guiding center approximation. However, this is limited to particles that are released in the periapse of the orbit. The guiding center approximation is applicable if the charge-to-mass ratio and the magnetic field strength of the star are large enough. Under these restrictions, the initial acceleration can give an indication of whether the dust particles are trapped or not.

For Vega and Fomalhaut, the main aim is to find if there were any bound trajectories for charged particles and, if yes, what they look like. The initial radial acceleration estimated in the guiding center approximation points outward for any reasonable initial values, predicting that no charged particles will be trapped even if the β-value is as low as 0.1, as shown in Fig. 3.

The only region where the guiding center is accelerated inward is closer than 0.02 AU from Vega and 0.025 AU from Fomalhaut. This is one to two star radii from the respective stellar surface, where the Parker model is not applicable. However, dust particles so close to the stars would probably be sublimated very quickly. Myrvang (2018) presented sublimation lifetimes for dust with different sizes and compositions at 0.3 AU. For most of the

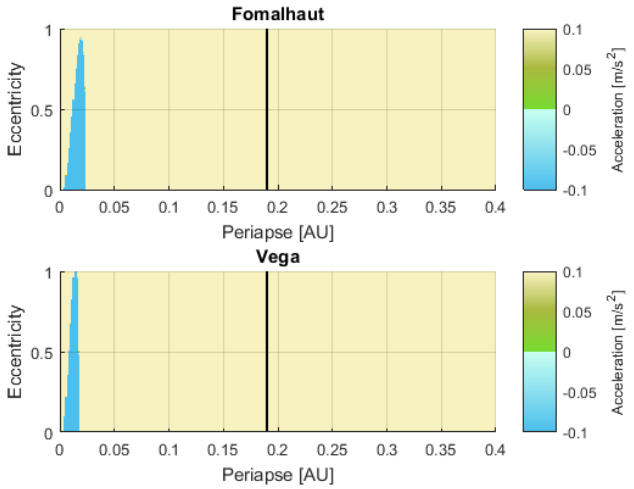

Fig. 3. Initial radial acceleration around Fomalhaut (*top*) and Vega (*bottom*) averaged over one gyroperiod by using the guiding center approximation. The black lines show the Alfvén radius. Both the x- and y-axis in the plot show values of the initial orbit. In order to compare with the situation in Fig. 2b for the Sun, $\beta = 0.1$.

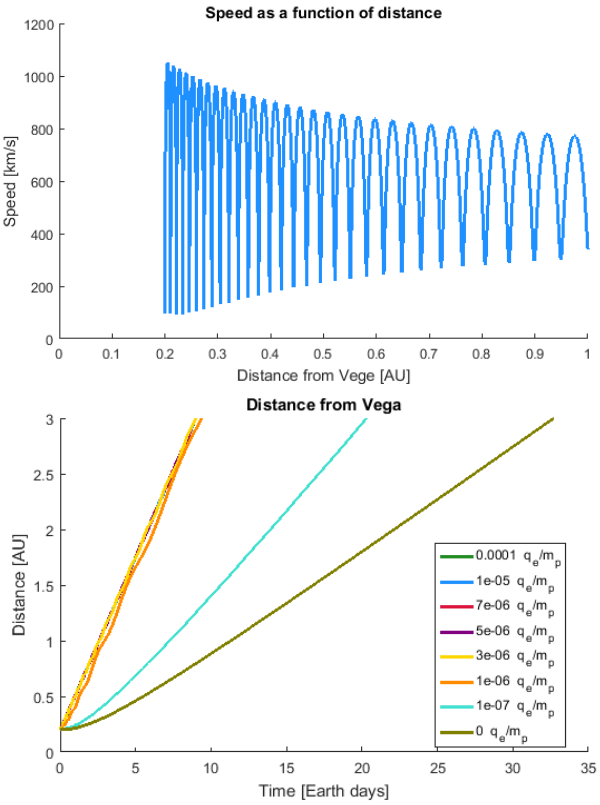

Fig. 4. Speed (*top*) and distance (*bottom*) of ejected particles from Vega. The trajectory calculations were made using $\beta = 2$. Uncertainties within β do not influence the dust trajectory. The particles are released from a circular orbit with radius = 0.1 AU and inclination of 5°. The top figure shows the speed of a single charged particle with charge-to-mass ratio $10^{-5}\ q_e/m_p$. The bottom figure shows the distance from Vega. The orbits of the particles with a charge-to-mass ratio of at least $1 \times 10^{-6} q_e/m_p$ are overlapping, as in Fig. 1.

materials that were considered, particles with a size of 100 nm or less sublimate within seconds already at 0.3 AU. Closer to the star, the sublimation lifetime will be even shorter. When β is as high as 2, that is, for small particle sizes, all particles are ejected in any case.

In order to investigate why the potential trapping zone is closer around Vega and Fomalhaut than around the Sun, we consider Eq. (8). The gravitation force of Vega and Fomalhaut is stronger than around the Sun. This probably only has a small effect since the larger gravitation also is taken into account in the initial values, because the particles are released from Keplerian orbits.

Due to the faster rotation of Fomalhaut and especially Vega, the magnetic field lines are much more closely wound and thus the magnetic field lines are almost azimuthal. This extends the region where the stellar wind velocity is perpendicular to the magnetic field closer to the stars.

The region where the magnetic mirror force is small is narrow and very close to the stars. It overlaps with the region where the total acceleration points inward. Here, the particle velocity and the stellar wind speed, both perpendicular to the magnetic field, are very similar. Also, in the last two terms, the acceleration is larger than for the Sun due to the faster stellar rotation. The stellar wind velocity is almost equal to the solar wind velocity and therefore does not contribute strongly to the shrinking of the trapping zone. Together the contributions sum up to a strong outward acceleration.

In addition to the acceleration along the magnetic field lines, the velocity perpendicular to the magnetic field is almost constant. In the regions where the magnetic field is more radial, this may not influence the orbits very much. The dust trajectory calculations for the Sun were done for this region. There, the magnetic field strength in radial and azimuthal directions cross at about 1 AU. Around Vega and Fomalhaut this happens closer to the star, so the magnetic field lines are already almost azimuthal at ~0.05 AU. The particles are then travelling outward with an almost constant speed.

A result of this can be seen in Fig. 4. Here, the time variation of the speed of a particle with charge-to-mass ratio $10^{-5}\ q_e/m_p$ is shown. The particle is accelerated to stellar wind speed almost immediately, although the speed oscillates strongly in the beginning. The oscillation frequency varies proportional with q/m-ratio. It also decreases with distance, indicating that this is due to the gyro-motion around a magnetic field line. The amplitude of these oscillations seems to be independent of the charge-to-mass ratio for high charge-to-mass ratios. The same pattern appears for other charge-to-mass ratios over $10^{-6}\ q_e/m_p$. Below this value, the particles do not reach the stellar wind speed.

Our simulations for Vega and Fomalhaut show that dust particles only stay in bound orbits if they are uncharged and the radiation pressure force is smaller than the gravitational force ($\beta < 1$). The dust that carries a large charge ($q/m \gtrsim 10^{-6}\ q_e/m_p$) is accelerated to the stellar wind speed (Fig. 4) and approaches this almost at once, within a few gyroperiods.

The Parker model has a limitation in that it does not describe the innermost region around the Sun correctly, that is, the area inside of the Alfvén radius. The dust belts around Vega and Fomalhaut are assumed to be at about this distance. We expect that our results would hold in case of open magnetic field lines.

The escaping charged particles with $q/m \geq 10^{-7} q_e/m_p$ approach stellar wind speed, which is much larger than the escape speed at the same distance. Due to this high speed, the particles pass 1 AU after approximately three days and 3 AU after seven days. We expect that in general, escaping charged particles have that behavior. The particles with $q/m \leq 10^{-7} q_e/m_p$

pass 3 AU after ~20–60 days, depending on initial conditions. Through collisions with dust and planetesimals further out, a stream of charged particles might affect the evolution of the debris disk over time. We note that for the β Pictoris debris disk, the influence of ejected particles on the collisional evolution of the debris disk was found to be considerable (Czechowski & Mann 2007).

6. Effects of plasma corotation

In the vicinity of the rotating star, the plasma is expected to corotate. To investigate the effect of plasma corotation on the magnetic field and the dynamics of the charged grains, we consider the following simple model. We let the plasma velocity and magnetic field components depend only on r and θ, with latitudinal components equal to zero. The azimuthal velocity component we assume to vary from the (approximate) surface rotation velocity of the star $\Omega R \sin\theta$ at the stellar surface to zero for $r \geq r_A$, where r_A is the Alfvén radius and R is the radius of the star. In particular, we consider the case of linear dependence:

$$u_\varphi(r,\theta) = \Omega R \sin\theta \frac{r_A - r}{r_A - R} \quad (r < r_A). \tag{10}$$

The magnetic field, apart from $\nabla \cdot \boldsymbol{B} = 0$, is assumed to satisfy the freezing-in equation

$$\nabla \times (\boldsymbol{u} \times \boldsymbol{B}) = 0, \tag{11}$$

with the boundary condition $B_\varphi = 0$ at $r = R$. The solution is

$$B_r(r,\theta) = b(\theta)/r^2, \tag{12}$$

and

$$B_\phi(r,\theta) = -\frac{\Omega b(\theta)\sin\theta}{u_r(r,\theta) r}\left[1 - \frac{u_\varphi(r,\theta)}{\Omega r \sin\theta}\right]. \tag{13}$$

In the calculations referred to in the present section, we assumed for simplicity that b and $u_r(r)$ do not depend on θ. For the radial velocity profile we have considered two cases: u_r = const. and the analytical model used in Czechowski & Mann (2018)

$$u_r(r) = \frac{f(r)}{1 + f(r)/C}, \tag{14}$$

with $f(r) = (2a(r - r_0))^{1/2}$, where $a = 3.4\ \mathrm{m\,s^{-2}}$, $r_0 = -0.6\,R$, and C = 800 km s^{-1}. For Vega and Fomalhaut, the stellar wind speed is multiplied by the escape velocity at the equator relative to the Sun and the stellar equator radius is inserted for R.

The model is used to calculate numerically the trajectories of charged dust grains for different initial conditions. We compare the results with those obtained with the Parker model described in Sect. 2. A comparison with the same initial conditions as in Fig. 1 is shown in Fig. 5. We find very little effect on trapped grain trajectories. In particular, the outer and lower limits in r are practically unaffected. The most prominent effect is a small shift in the period of radial oscillations observed for r-dependent u_r (Eq. (14)).

Our calculations include the initial distances between 0.15 and 0.01 AU; that is close to the upper limit and well inside the trapping region for the Sun. We also assume different values of the Alfvén radius (0.1 and 0.15 AU for the case of the Sun).

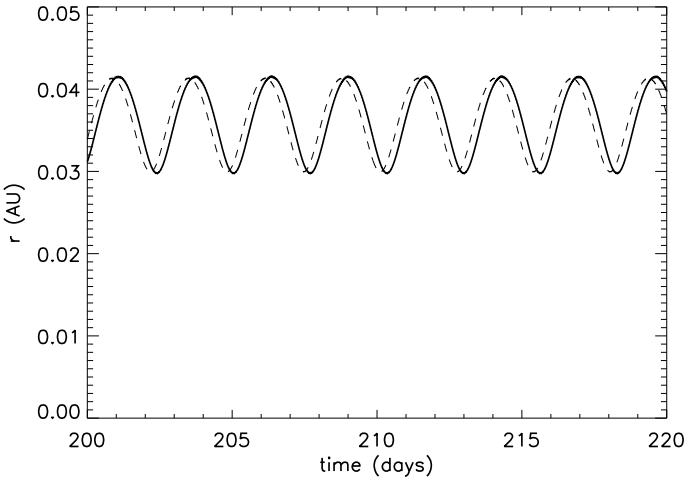

Fig. 5. Effect of corotation on trapped particle trajectory. Particles with a charge-to-mass ratio $10^{-5}\ q_e/m_p$ are released from a circular orbit of radius 0.04 AU and inclination of 5°. The solid (dashed) lines show the distance from the Sun along the trajectories corresponding to the cases without (with) corotation. The radial velocity profile given by Eq. (14) is used. The particles are emitted at $t = 0$, but the difference in phase between the trajectories is visible only at later times.

For $\beta = 0.1$, charged particles around Vega and Fomalhaut initially accelerate inward if released close enough to the star as predicted by the guiding center approximation (Eq. (8) and Fig. 3). Close to the equator, the particles fall into the star after some hours, but for highly inclined initial orbits, there exist trapped trajectories similar to those for the Sun. However, at these distances, small particles would sublimate within a short amount of time (see Sect. 5). On the other side, a particle for which the ratio between radiation and gravity force is 0.1 has a size that is larger than ~10 μm (Myrvang 2018). For charging conditions in the solar system and around A-class stars, this corresponds to a charge-to-mass ratio of less than $10^{-11} q_e/m_p$. Therefore, it could be that such particles can be treated as uncharged.

We conclude that trapping of charged dust is not precluded by the partly corotating corona, at least for the case when the magnetic field is frozen in the plasma flow, and the latitudinal flow is absent. We leave a more complete study of the effect of plasma corotation on charged dust dynamics to a separate work.

7. Conclusion

This paper presents the model calculations of dust trajectories in a Parker-type magnetic field close to the Sun, Vega, and Fomalhaut. The considered acting forces are gravitation, radiation pressure, and Lorentz force. In the initial conditions, the following parameters are modified: semimajor axis, eccentricity, inclination, and true anomaly and they lead to different results that we discuss. The charge and mass of the dust particles enter the calculations as the ratio of surface charge to mass, which we vary over a range of parameters for dust of different sizes. When the charge-to-mass ratio exceeds $10^{-6}\ q_e/m_p$, the particles move on similar trajectories independent of the charge-to-mass ratio. This corresponds to approximate particle sizes of 30 nm and smaller for charging conditions in the solar system and around A-type stars.

The calculations show that charged particles are generally not trapped around Vega and Fomalhaut, but rather ejected. The

ejected particles reach the stellar wind speed almost instantaneously (see Fig. 4). This is different from the solar system, where previous works (Czechowski & Mann 2010) have shown that under certain initial conditions the charged particles are trapped in the vicinity of the Sun. Those particles that are ejected from the vicinity of the Sun do not necessarily reach the solar wind speed or only after a long time.

We find that the dust trapping and dust ejection conditions in the Parker-type magnetic field depend on the form of the magnetic field, which is determined by the stellar rotation speed and the stellar wind speed. The particles are ejected more quickly when the stellar rotation is slower and the stellar wind is faster. In solar conditions, the trapping occurs outward to around 0.25 AU. Vega and Fomalhaut rotate ~10–100 times faster than the Sun, and as a result the trapping zone moves very close to the star and the dust particles are ejected more quickly. A potential trapping zone could form inside of 0.02 AU for Vega and 0.025 AU for Fomalhaut, if radiation pressure force were smaller than gravity force and the Parker field approximation still applicable. We also note that sublimation lifetimes are short that close to the stars.

Particle trajectories are less affected by the Lorentz force when the charge-to-mass ratio is smaller than $10^{-7} q_e/m_p$, that is, for particles larger than 100 nm. In the case of Vega and Fomalhaut, these particles are ejected because the radiation pressure force exceeds gravity. In case of the Sun, the radiation pressure force can be smaller than the gravitational force and the exact conditions for bound or unbound orbits depend on the initial orbits and on the location within the orbit where the dust particle is released.

We find that the initial acceleration of a particle derived under the guiding center approximation can serve as a criterion to predict whether a particle is trapped or not, as long as the particle is released in the periapsis of the initial orbit. The guiding center approximation is found to be applicable for charge-to-mass ratios $q/m \geq 10^{-5} q_e/m_p$ (Czechowski & Mann 2010), that is, for dust particles with sizes of few nanometers. The trapping arises in a Parker-type magnetic field, which may also include the effect of plasma corotation. This is different from the model assumptions of a recent work by Rieke et al. (2016) where the dust trajectories are studied in a dipole field. Our study of the dust trajectories is also different from a study by Kimura et al. (2018) who concentrate on dust destruction and charging processes.

In summary, we find from our calculations no trapping of dust particles around Vega and Fomalhaut as long as the radiation pressure force exceeds the gravitational force. The particles that are predominantly influenced by electromagnetic force (of a size smaller than 100 nm) stay within a 3 AU distance of Fomalhaut for less than approximately seven days and within 3 AU distance of Vega for less than approximately seven days. The particles that are predominantly influenced by radiation pressure force (of size 100 nm and larger) stay within 3 AU distance of the stars for typically 20–60 days. The results of our calculations do not support the hypothesis (Su et al. 2013) that the hot dust emission at Vega and Fomalhaut is produced by nanodust in trapped orbits near the stars. Dust particles that form in the inner debris disks in the vicinity of the stars do contribute to the observed thermal emission brightness, but only for a short time, so that a high rate of dust production in the inner disks of Vega and Fomalhaut is needed to explain the observational data with dust emission. Finally, the escaping particles can play a role in the evolution of the outer debris disks.

Acknowledgements. We thank the referee, Jens Kleimann, for his thorough review and helpful suggestions, which improved the paper. Work presented is also the subject of the Master thesis projects of J.S. and M.M. at the Department of Physics and Technology at UiT. The work is supported by the Research Council of Norway (grant number 262941). J.S. carried out the trajectory calculations and prepared the manuscript. C.B. supported the preparation of the numerical codes, made calculations with an independent code for comparison and provided parameters on the dust destruction. A.C. provided his own code for dust in the solar system that was used as a benchmark and gave advice on the trajectory calculations and on dynamics in general. M.M. prepared the estimates of the radiation pressure force that was used in the calculations. I.M. suggested the topic and outline of the work and supervised the thesis projects. All authors discussed the work together during the project and participated in preparing the manuscript. Thanks to Åse Mari for help in preparing the manuscript and Norsk Romsenter for travel support to present and discuss these results.

References

Absil, O., di Folco, E., Augereau, J., et al. 2006, A&A, 452, 237
Absil, O., Mennesson, B., Le Bouquin, J.-B., et al. 2009, ApJ, 704, 150
Absil, O., Defrère, D., Coudé du Foresto, V., et al. 2013, A&A, 555, A104
Bonanno, A., Schlattl, H., & Paternò, L. 2002, A&A, 390, 1115
Braithwaite, J., & Cantiello, M. 2013, MNRAS, 428, 2789
Czechowski, A., & Kleimann, J. 2017, Ann. Geophys., 35, 1033
Czechowski, A., & Mann, I. 2007, ApJ, 660, 1541
Czechowski, A., & Mann, I. 2010, ApJ, 714, 89
Czechowski, A., & Mann, I. 2011, ApJ, 732, 127
Czechowski, A., & Mann, I. 2012, in Nanodust in the Solar System: Discoveries and Interpretations, eds. I. Mann, N. Meyer-Vernet, & A. Czechowski, Astrophys. Space Sci. Lib. (Heidelberg: Springer), 385
Czechowski, A., & Mann, I. 2018, A&A, 617, A43
Defrère, D., Absil, O., Augereau, J.-C., et al. 2011, A&A, 534, A5
Díaz, C. G., González, J. F., Levato, H., & Grosso, M. 2011, A&A, 531, A143
Ertel, S., Defrere, D., Absil, O., et al. 2016, A&A, 595, A44
Hakamada, K., & Kojima, M. 1994, Sol. Phys., 153, 419
IAU 2015, IAU 2015 Resolution B3 on Recommended Nominal Conversion Constants for Selected Solar and Planetary Properties., Tech. Rep., IAU Inter-Division A-G Working Group on Nominal Units for Stellar & Planetary Astronomy
Kimura, H., Kunimoto, M., Suzuki, T. K., et al. 2018, Planet. Space Sci. DOI: https://doi.org/10.1016/j.pss.2018.07.010
Köhler, M., & Mann, I. 2002, in Proceedings of Asteroids, Comets, Meteors – ACM 2002, ed. B. Warmbein (Noordwijk: ESA Publications Division), 771
Lammer, H., Bredehöft, J., Coustenis, A., et al. 2009, A&ARv, 17, 181
Lebreton, J., van Lieshout, R., Augereau, J.-C., et al. 2013, A&A, 555, A146
Lignières, F., Petit, P., Böhm, T., & Aurière, M. 2009, A&A, 500, 41
Mamajek, E. E. 2012, ApJ, 754, 2
Mann, I., Murad, E., & Czechowski, A. 2007, Planet. Space Sci., 57, 1000
Moro-Martin, A. 2013, Dusty Planetary Systems, eds. T. D. Oswalt, L. M. French, & P. Kalas (Dordrecht: Springer), 431
Myrvang, M. 2018, Master thesis, Universitetet i Tromsø, Norway
Northrop, T. G. 1963, The Adiabatic Motion of Charged Particles (New York: John Wiley & Sons, Ltd.)
Parker, E. N. 1958, ApJ, 128, 664
Rieke, G. H., Gáspár, A., & Ballering, N. P. 2016, ApJ, 816, 50
Schatten, K. H., Wilcox, J. M., & Ness, N. F. 1969, Sol. Phys., 6, 442
Sezestre, É., Augereau, J.-C., Boccaletti, A., & Thébault, P. 2017, A&A, 607, A65
Su, K. Y. L., Rieke, G. H., Malhotra, R., et al. 2013, ApJ, 763, 2
Wyatt, M. C. 2009, in Small Bodies in Planetay Systems, eds. I. Mann, A. M. Nakamura, & T. Mukai, Astrophys. Space Sci. Lib. (Berlin: Springer), 385
Yoon, J., Peterson, D. M., Kurucz, R. L., & Zagarello, R. J. 2010, ApJ, 708, 71